

1 **Multiobjective sensitivity analysis and optimization of a**
2 **distributed hydrologic model MOBIDIC**

3
4 Jing Yang^{*1}, Fabio Castelli², Yaning Chen¹

5
6 ¹State Key Laboratory of Desert and Oasis Ecology, Xinjiang Institute of Ecology and
7 Geography, Chinese Academy of Sciences, Xinjiang, 830011, China

8
9 ²Department of Civil and Environmental Engineering, University of Florence, Italy

10
11
12 ***Corresponding author:**

13 Jing Yang

14 State Key Laboratory of Desert and Oasis Ecology, Xinjiang Institute of Ecology and
15 Geography, Chinese Academy of Sciences, Xinjiang, 830011, China

16 Tel: +86-991-7823171

17 Email: yangjing@ms.xjb.ac.cn

18 **Abstract**

19 Calibration of distributed hydrologic models usually involves how to deal with the large
20 number of distributed parameters and optimization problems with multiple but often
21 conflicting objectives which arise in a natural fashion. This study presents a
22 multiobjective sensitivity and optimization approach to handle these problems for a
23 distributed hydrologic model MOBIDIC, which combines two sensitivity analysis
24 techniques (Morris method and State Dependent Parameter method) with a multiobjective
25 optimization (MOO) approach ϵ -NSGAII. This approach was implemented to calibrate
26 MOBIDIC with its application to the Davidson watershed, North Carolina with three
27 objective functions, i.e., standardized root mean square error of logarithmic transformed
28 discharge, water balance index, and mean absolute error of logarithmic transformed flow
29 duration curve, and its results were compared with those with a single objective
30 optimization (SOO) with the traditional Nelder-Mead Simplex algorithm used in
31 MOBIDIC by taking the objective function as the Euclidean norm of these three
32 objectives. Results show: 1) The two sensitivity analysis techniques are effective and
33 efficient to determine the sensitive processes and insensitive parameters: surface runoff
34 and evaporation are very sensitive processes to all three objective functions, while
35 groundwater recession and soil hydraulic conductivity are not sensitive and were
36 excluded in the optimization; 2) Both MOO and SOO lead to acceptable simulations, e.g.,
37 for MOO, average Nash-Sutcliffe is 0.75 in the calibration period and 0.70 in the
38 validation period; 3) Evaporation and surface runoff shows similar importance to
39 watershed water balance while the contribution of baseflow can be ignored; 4) Compared
40 to SOO which was dependent of initial starting location, MOO provides more insight on

41 parameter sensitivity and conflicting characteristics of these objective functions.

42 Multiobjective sensitivity analysis and optimization provides an alternative way for

43 future MOBIDIC modelling.

44

45 **Keywords**

46 Multiobjective optimization, sensitivity analysis, distributed hydrologic model, model

47 calibration

48 **1. Introduction**

49 With the development of information technology (e.g., high performance computing
50 cluster and remote sensing technology), there has been a prolific development of
51 integrated, distributed and physically-based watershed models (e.g., MIKE-SHE,
52 Refsgaard and Storm, 1995) over the past two decades, which are increasingly being used
53 to support decisions about alternative management strategies in the areas of land use
54 change, climate change, water allocation, and pollution control. Though in principle
55 parameters of distributed and physically based models should be assessable from
56 catchment data (in traditional conceptual rainfall-runoff models, parameters are obtained
57 through a calibration process), these models still need a parameter calibration process in
58 practice due to scaling problems, experimental constraints, etc. (Beven and Binley, 1992;
59 Gupta et al, 1998; Madsen, 2003). Problems, arising in calibrating distributed hydrologic
60 models, include how to handle large number of distributed parameters and optimization
61 problems with multiple but often conflicting objectives.

62

63 In the literature, to deal with large number of distributed model parameters, this is often
64 done by aggregating distributed parameters (e.g., Yang et al., 2007), or screening out the
65 unimportant parameters through a sensitivity analysis (e.g., Muleta and Nicklow, 2005;
66 Yang, 2011). Sensitivity analysis can be used to not only screen out the most insensitive
67 parameters, but also study the system behaviors identified by parameters and their
68 interactions, qualitatively or quantitatively. However, most of applications in
69 environmental modelling are based on the one-at-a-time (OAT) local sensitivity analysis,
70 which is “predicated on assumptions of model linearity which appear unjustified in the

71 cases reviewed” (Saltelli and Annoni, 2010), or simple linear regressions where a lot of
72 uncertainty are not fairly accounted for. The use of global sensitivity analysis techniques
73 is very crucial in distributed modelling. Only recently, global sensitivity analysis
74 techniques and multiobjective sensitivity analysis started to appear in hydrologic
75 modelling, and van Werkhoven et al (2009) demonstrates how the calibration result
76 responds to reduced parameter sets with different objectives and different metrics of
77 parameter exclusion.

78

79 Although most hydrologic applications are based on the single objective calibration,
80 model calibration with multiple and often conflicting objectives arises in a natural fashion
81 in hydrologic modelling. This is not only due to the increasing availability of multi-
82 variable (e.g., flow, groundwater level, etc.) or multi-site measurements, but also due to
83 the intrinsic different system responses (e.g., peaks and baseflow in the flow series).
84 Instead of finding a single optimal solution in the single objective optimization (SOO),
85 the task in the multiobjective optimization (MOO) is to identify a set of optimal trade-off
86 solutions (called a Pareto set) between conflicting objectives. Although there are
87 criticisms of MOO such as that only one parameter set can be used for decision making,
88 recently researches (e.g., Kollat and Reed, 2007) start to provide the answers. In
89 hydrology, the traditional method to solve multiobjective problems is to form a single
90 objective, e.g., by giving different weights to these multiple objectives or applying some
91 transfer function. Over the past decade, several MOO algorithms approaches have been
92 applied to the conceptual rainfall-runoff models (e.g., Yapo et al., 1998; Gupta et al.,
93 1998, Madsen, 2000, Boyle et al., 2000; Vrugt et al., 2003; Liu and Sun, 2010), and now

94 increasing applied to distributed hydrologic models (e.g., Madsen, 2003; Bekele and
95 Nicklow, 2007; Shafii and Smedt, 2009; MacLean et al., 2010). And there are some
96 papers (Tang et al., 2006; Wöhling et al., 2008) to comparatively study their strengths
97 with the application in hydrology. A good review of MOO applications in hydrological
98 modelling is given by Efstratiadis and Koutsoyiannis (2010). It is worth noting that the
99 multiobjective calibration is different from statistical uncertainty analysis which is based
100 on the concept (or similar concept) of “equifinality” (see discussion in Gupta et al., 1998,
101 and Boyle et al., 2000).

102

103 This paper applies two sensitive analysis techniques (Morris method and State Dependent
104 Parameter method) and ϵ -NSGAI in the multiobjective sensitive analysis and calibration
105 framework. This was implemented to calibrate a distributed hydrological model
106 MOBIDIC with its application to the Davidson watershed, North Carolina. The purpose
107 is to study parameter sensitivity of the hydrologic model MOBIDIC and explore the
108 capability of MOO in calibrating the MOBIDIC compared to the traditional SOO used in
109 MOBIDIC applications.

110

111 This paper is structured as follows: section 2 gives a description of the MOBIDIC model;
112 section 3 introduces the approach in the multiobjective sensitivity analysis and
113 optimization; section 4 gives a brief introduction of the study site, model setup, objective
114 selection, and sensitivity and calibration procedure; in section 5, the results are presented
115 and discussed; and finally the main results are summarized and conclusions are drawn in
116 ‘conclusions’ section.

117

118 2 Hydrologic model MOBIDIC

119 MOBIDIC (MOdello di Bilancio Idrologico DIstribuito e Continuo; Castelli et al., 2009;
120 Campo et al., 2006) is a distributed and raster-based hydrological balance model.
121 MOBIDIC simulates the energy and water balances on a cell basis within the watershed.
122 Figure 1 gives a schematic representation of MOBIDIC. The energy balance is
123 approached by solving the heat diffusion equations in multiple layers in the soil-
124 vegetation system, while the water balance is simulated in a series of reservoirs (i.e.,
125 boxes in Figure 1) and fluxes between them.

126

127 For each cell, water in the soil is simulated by

$$\begin{aligned} \frac{dW_g}{dt} &= I_{nf} - S_{per} - Q_d - S_{as} \\ \frac{dW_c}{dt} &= S_{as} - E_t \end{aligned} \quad (1)$$

129 where W_g [L] and W_c [L] are the water contents in the soil gravitational storage and
130 capillary storage, respectively, and I_{nf} [LT^{-1}], S_{per} [LT^{-1}], Q_d [LT^{-1}], E_t [LT^{-1}], and S_{as}
131 [LT^{-1}] are infiltration, percolation, interflow, evaporation, and adsorption from
132 gravitational to capillary storage, which are modeled through following equations:

$$133 \quad S_{per} = \gamma \cdot W_g$$

$$134 \quad Q_d = \beta \cdot W_g$$

$$135 \quad S_{as} = \kappa \cdot (1 - W_c / W_{c,max}) \quad (2)$$

$$I_{nf} = \begin{cases} \left[P + (Q_d + Q_h + R_d)_{up} \right] \left[1 - \exp \left(\frac{-K_s}{P + (Q_d + Q_h + R_d)_{up}} \right) \right] & \text{if } W_g < W_{g,max} \\ 0 & \text{otherwise} \end{cases}$$

136 where γ , β and κ are percolation coefficient [T^{-1}], interflow coefficient [T^{-1}], and soil
137 adsorption coefficient [LT^{-1}], respectively, P the precipitation [LT^{-1}], Q_h and R_d Horton
138 runoff and Dunne runoff, K_s the soil hydraulic conductivity [LT^{-1}], W_{gmax} [L] and W_{cmax}
139 [L] the gravitational and capillary storage capacities.

140

141 Once the surface runoff (Q_h and R_d) and baseflow are calculated, three different methods
142 can be used for river routing, i.e., the lag method, the linear reservoir method,
143 Muskingum-Cunge method (Cunge, 1969). Muskingum-Cunge method was used in this
144 study.

145

146 MOBIDIC uses either a linear reservoir or the Dupuit approximation to simulate the
147 groundwater balance which relates the groundwater change to the percolation, water loss
148 in aquifers and baseflow. In this case study, the linear reservoir method was used.

149

150 Although there are many distributed parameters in MOBIDIC, normally these distributed
151 parameters are calibrated through the “aggregate” factors (e.g., the multiplier for
152 hydraulic conductivity) based on their initial estimations. And hereafter we use the term
153 “factor” (instead of “model parameter”) when we conduct the sensitivity analysis and
154 optimization, to avoid the confusion with the term “model parameter” used in model
155 description. A factor can be a model parameter or a group of distributed model
156 parameters with the same parameter name, and in this paper it is a change to be applied to
157 a group of model parameters. In MOBIDIC, normally nine factors (i.e., nine groups of
158 parameters) need to be calibrated. These factors, their explanations, and their
159 corresponding model parameters are listed in Table 1.

160

161 **3 Methodology**

162 The procedure applied here consists of two-step analyses, i.e., a multiobjective sensitivity
163 analysis generally characterizing the basic hydrologic processes and single out the most
164 insensitive factors, and a multiobjective calibration aiming at trade-offs between different
165 objective functions.

166 *3.1 Sensitivity analysis techniques*

167 Sensitivity analysis is to assess how variations in model out can be apportioned,
168 qualitatively or quantitatively, to different sources of variations, and how the given model
169 depends upon the information fed into it (Saltelli et al., 2008). In the literature, a lot of
170 sensitivity analysis methods are introduced and applied, e.g., Yang (2011) applied and
171 compared five different sensitivity analysis methods. Here we adopted an approach which
172 combines two global sensitivity analysis techniques, i.e., the Morris method (Morris,
173 1991) and SDP method (Ratto et al., 2007).

174 *3.1.1 Morris method*

175 Morris method is based on replicated and randomized one-factor-at-a-time design (Morris,
176 1991). For each factor X_i , Morris method uses two statistics, μ_i and σ_i , which measure the
177 degree of factor sensitivity, and the degree of nonlinearity or factor interaction,
178 respectively. The higher μ_i is, the more important the factor X_i is to the model output; and
179 the higher σ_i is, the more nonlinear the factor X_i is to the model output or more
180 interactions with other factors (details refer to Morris, 1991; Campolongo et al., 2007).
181 Morris method takes $m*(n+1)$ model runs to estimate these two sensitivity indices for
182 each of n factors with sample size m . The advantage is it is efficient and effective to
183 screen out insensitive factors. Normally m takes values around 50. And according to

184 Saltelli et al. (2008), the sensitivity measure (μ_i) is a good proxy for the total effect (i.e.,
185 S_{Ti} in Eq. 4 below), which is a robust measure in sensitivity analysis.

186

187 3.1.2 State-Dependent Parameter method (SDP)

188 SDP (Ratto et al., 2007) is based on the ANOVA functional decomposition, which
189 apportions the model output uncertainty (100%, as 1 in Eq. 3) to factors and different
190 levels of their interactions:

$$191 \quad 1 = \sum_i S_i + \sum_i \sum_{j>i} S_{ij} + \dots + S_{12\dots n} \quad (3)$$

192 where S_i is the main effect of factor X_i representing the average output variance
193 reduction that can be achieved when X_i is fixed, and S_{ij} is the first-order interaction
194 between X_i and X_j , and so on. In ANOVA based sensitivity analysis, total effect (S_{Ti})
195 is frequently used, which stands for the average output variance that would remain as
196 long as X_i stays unknown,

$$197 \quad S_{Ti} = S_i + \sum_{j \neq i} S_{ij} + \dots + S_{12\dots n} \quad (4)$$

198 SDP method uses the emulation technique to approximate lower order sensitivity indices
199 in Eq. (3) (e.g., S_i and S_{ij} in this study) by ignoring the higher order sensitivity indices.

200 And we define $S_{Di} = S_i + \sum_j S_{ij}$ (referred to as “quasi total effect” later) as a surrogate to

201 the total effect. The advantage is that it can precisely estimate lower order sensitivity
202 indices at a lower computational cost (normally 500 model runs, which is independent of
203 number of factors). The disadvantage is that it cannot estimate higher order sensitivity
204 indices.

205

206 In practice, especially for over-parameterized cases, Morris method is firstly suggested to
207 screen out insensitive factors, and then SDP method is applied to quantify the
208 contributions of the sensitive factors and their interactions. In this study, as model
209 parameters are aggregated into nine factors (as listed Table 1), these two methods are
210 applied individually. And then, the sensitivity of each factor and its system behaviour
211 will be discussed, qualitatively by Morris method, and quantitatively by SDP method.
212 And then the most insensitive factors will be screened out and excluded in the calibration.

213

214 In the context of multiobjective analysis, sensitivity analysis applied includes: 1) to
215 examine the sensitivity of each factor to different objective functions, qualitatively or
216 quantitatively; 2) to single out the most sensitive factors and study the physical
217 behaviours of the system; 3) to exclude the most insensitive factors and therefore
218 simplify the process of calibration. It is worth noting: this sensitivity analysis approach
219 applied here is not a fully multiobjective sensitivity analysis approach as proposed by
220 Rosolem et al (2012 and 2013) which applies sensitivity analysis to all objectives in an
221 integrated way and is objective. However compared to the fully multiobjective sensitivity
222 analysis approach (as proposed in Rosolem et al, 2012) which easily requires over 10,000
223 model runs, our approach is very computationally efficient as both Morris method and
224 SDP method only need several hundred model runs, which is highly appreciable for
225 physically based and distributed hydrologic models.

226

227 *3.2 Multiobjective calibration and ϵ -NSGAI*

228 In the literature of hydrologic modelling, most applications are single objective based,
229 which aims at a single optimal solution. However, for example in flow calibration, there
230 is always a case that two solutions, one solution better simulates the peaks and poorly
231 simulates the baseflow while the other solution poorly simulates the peaks while better
232 simulates the baseflow. These two solutions, called Pareto solutions, are
233 incommensurable, i.e., better fitting of the peaks will lead to worse fitting of the baseflow,
234 and vice versa. This belongs to the domain of MOO, aiming at finding a set of optimal
235 solutions (Pareto solutions), instead of one single solution.

236
237 Generally a MOO problem can be formulated as follows:

$$\begin{aligned} 238 \quad \min F(X) &= (f_1(X), f_2(X), \dots, f_i(X), \dots, f_k(X)) \\ \text{s.t. } G(X) &= (g_1(X), g_2(X), \dots, g_i(X), \dots, g_l(X)) \end{aligned} \quad (5)$$

239 Where X is an n -dimensional vector and in this study represents the model factors to be
240 calibrated, $f_i(X)$ i^{th} objective function, and $g_i(X)$ i^{th} constraint function.

241
242 In the literature, there are many algorithms available to obtain the Pareto solutions, e.g.,
243 NSGAI (Non-dominated Sorting Genetic Algorithm-II; Deb et al, 2002), SPEA2
244 (Strength Pareto Evolutionary Algorithm 2; Zitzler et al., 2001), MOSCEM-UA
245 (Multiobjective Shuffled Complex Evolution Metropolis; Vrugt et al., 2003), and ϵ -
246 NSGAI (Kollat and Reed, 2006), etc. In this study, we adopt ϵ -NSGAI, which is
247 efficiency, reliability, and ease-of-use. Its strengths have been comparatively studied in
248 Kollat and Reed (2006) and Tang et al. (2006).

249

250 ϵ -NSGAI is an extension of the NSGAI (Deb et al., 2002), a second generation of
251 multiobjective evolution algorithm. The main characteristics of ϵ -NSGAI include: (i)
252 Selection, crossover, and mutation processes as other genetic algorithm by mimicking the
253 process of natural evolution, (ii) an efficient non-domination sorting scheme, (iii) an
254 elitist selection method that greatly aids in capturing Pareto front, (iv) ϵ -dominance
255 archiving, (v) adaptive population sizing, and (vi) automatic termination to minimize the
256 need for extensive parameter calibration. More details refer to Kollat and Reed (2006). In
257 this study, two changes were made to the original ϵ -NSGAI: 1) the initial population is
258 generated with Sobol' quasi-random sampling technique to improve the coverage of
259 parameter space; 2) the code is parallelized and interfaced with MOBIDIC to improve the
260 computational speed.

261

262 As a comparison, a single objective function is defined as 2-norm of the multiple
263 objectives $F(X)$, which measures how close to the original point (theoretical optimum O):

$$264 \quad sof = \|F(X)\|_2 = \sqrt{\sum_{i=1}^k f_i(X)^2} \quad (6)$$

265 And SOO was done with the classic Nelder–Mead algorithm (Nelder and Mead, 1965)
266 which is already coded into the MOBIDIC package.

267

268 To analyze the Pareto solution and also compare with the solution from SOO, except for
269 traditional methods, the “Level diagrams” proposed by Blasco et al. (2008) was also used.

270 Compared to traditional methods, it can visualize high dimensional Pareto front and
271 synchronizes the objective and factor diagrams. The procedure and includes two steps. In
272 the first step, the vector of objectives (k -dimension) for each Pareto point is mapped to a

273 real number (one-dimension) according to the proximity to the theoretical optimum
274 measured with a specific norm of objectives; and in the second step, these norm values
275 are plotted against the corresponding values of each objective or factor. 1-norm, 2-norm
276 and ∞ -norm are suggested. To compare with SOO, 2-norm was used.

277

278 **4 Davidson watershed and objective selection**

279 *4.1 Davidson watershed*

280 The Davidson watershed, located in southwest mountain area of North Carolina, drains
281 an area of 105km² above the station “Davidson river near Brevard” (see Figure 2). The
282 elevation ranges from 645m to 1,820m above sea level. Based on the NLDAS climate
283 data, the average annual precipitation is 1,900mm and varies from 1,400mm to 2,500mm,
284 and daily temperature changes from -19°C to 26°C. The average daily flow is about
285 3.68m³/s.

286

287 Data used in MOBIDIC model include (i) Digital Elevation Model (DEM), (ii) soil data,
288 (iii) land cover data, (iv) climate data (precipitation, minimum and maximum temperature,
289 solar radiation, humidity and wind speed), and (v) flow data. 9m DEM, land cover,
290 SSURGO soil data, one station (Davidson river near Brevard) of flow data are from U.S.
291 Geological Survey, and hourly NLDAS climate data from National Aeronautics and
292 Space Administration (NASA). NLDAS integrates a large quantity of observation-based
293 and model reanalysis data to drive offline (not coupled to the atmosphere) land-surface
294 models (LSMs), and executes at 1/8th-degree grid spacing over central North America,
295 enabled by the Land Information System (LIS) (Kumar et al., 2006; Peters-Lidard et al.,
296 2007).

297

298 DEM is used to delineate the watershed and estimate the topographic parameters and
299 river system, Land cover for evaporation parameters, soil data for soil parameters,
300 climate data is used to drive MOBIDIC, and flow data are used to calibrate the model and
301 assess model performance. The climate and flow data used in this study are from Jan 1,
302 1996 to Sep 30, 2006. As NLDAS only has hourly temperature daily instead of hourly
303 minimum and maximum temperature needed by MOBIDIC, we compiled the hourly
304 climate data to daily data and run the model at a daily step. After MOBIDIC setup, the
305 initial parameter values are listed in third column of Table 1.

306

307 We split the data into a warm-up period (from Jan 1, 1996 to Sep 30, 2000), a calibration
308 period (from Oct 1, 2000 to Sep 30, 2003), and a validation period (from Oct 1, 2003 to
309 Sep 30, 2006).

310

311 *4.2 Objective function selection*

312 After setting up MOBIDIC in the Davidson watershed, three objective functions were
313 used in the multiobjective sensitivity analysis and optimization:

314 1) Standardized root mean square error between the logarithms of simulated and observed
315 outflows:

$$316 \quad SRMSE = \frac{\sqrt{\frac{1}{N} \sum_{i=1}^N (\log(Q_i^{obs}) - \log(Q_i^{sim}))^2}}{\sqrt{\frac{1}{N-1} \sum_{i=1}^N (\log(Q_i^{obs}) - \overline{\log Q})^2}} \quad (7)$$

317 2) Water Balance Index, calculated as the mean absolute error between the simulated and
318 observed flow accumulation curves:

$$319 \quad WBI = \frac{1}{N} \sum_{i=1}^N |Q_{Ci}^{obs} - Q_{Ci}^{sim}| \quad (8)$$

320 3) Mean absolute error between the logarithms of simulated and observed flow duration
321 curves

322 $MARD = \frac{1}{100} \sum_{i=1}^N | \log(Q_{Pi}^{obs}) - \log(Q_{Pi}^{sim}) |$ (9)

323 In Eq. (7), (8) and (9), Q_i^{obs} and Q_i^{sim} are observed and simulated flow series at time step i ,

324 N the data length, $\overline{\log Q}$ the average of logarithmic transformed observed flows, Q_{Ci}^{obs} and

325 Q_{Ci}^{sim} i^{th} observed and simulated accumulated flows, and Q_{Pi}^{obs} and Q_{Pi}^{sim} i^{th} percentiles of

326 observed and simulated flow duration curves.

327 $SRMSE$ (Eq. 7), WBI (Eq. 8), and $MARD$ (Eq. 9) are measures of the closeness between

328 simulated and observed flow series, water balance, and closeness between simulated and

329 observed flow frequencies, respectively. The smaller these measures are, the better the

330 simulation is, and the minima are (0, 0, 0) meaning a perfect match between the

331 simulation and observation. It is worth noting that we use the logarithms of the flows

332 instead of flows to avoid overfitting flow peaks (Boyle et al., 2000; Shafii and De Smedt,

333 2009) as flood forecasting is not our main focus. And for $SRMSE$, we have $NS \approx 1 -$

334 $SRMSE^2$ when N is large (e.g., > 100), where NS is the Nash-Sutcliffe coefficient (Nash

335 and Sutcliffe, 1970), which is widely used in hydrologic modelling.

336 And accordingly, the single objective function here is the Euclidean norm (2-norm) of

337 $SRMSE$, WBI , and $MARD$:

338 $sof = \sqrt{SRMSE^2 + WBI^2 + MARD^2}$ (10)

339

340 **5 Result and discussion**

341 *5.1 Multiobjective sensitivity analysis*

342 Morris method and SDP method were applied individually to the initially selected factors

343 (in Table 1).

344 For Morris method, its convergences for three objective functions, monitored using the
345 method proposed in Yang (2011), were achieved around 700~800 model simulations.
346 Figure 3 gives the sensitivity results for objective functions *SRMSE*, *WBI*, and *MARD*,
347 respectively. In each plot, the horizontal axis (μ) denotes the degree of factor sensitivity,
348 and the vertical axis (σ) denotes the degree of factor nonlinearity or interaction with other
349 factors.

350 For *SRMSE*, the most sensitive factors are group ($p\alpha$, $p\gamma$, and $p\kappa$), followed by $p\beta$ and
351 rCH , while other factors (especially rK_s and rK_f) are not so sensitive. This applies to the
352 degree of the factor nonlinearity or interaction. Factors in the same group have a similar
353 effect on studied objective function. The sensitivities of $p\alpha$, $p\gamma$, and $p\kappa$ indicate the
354 importance of their corresponding processes (i.e., surface runoff, percolation, and
355 adsorption which is related to evapotranspiration) to *SRMSE*, while interflow ($p\beta$) is less
356 important and other processes/characteristics (e.g., groundwater flow, rK_f) are not
357 important.

358 For *WBI*, the dominating parameter is $p\kappa$, followed by $p\alpha$, $p\gamma$, $p\beta$ and rCH , while other
359 factors (especially rK_f and rW_{cmax}) are not so sensitive. *WBI* measures the water balance
360 between observed and simulated flow series, and it is reasonable that $p\kappa$ which controls
361 the water supply for evaporation is most sensitive while other factors ($p\alpha$, $p\gamma$, $p\beta$ and rCH)
362 are sensitive mainly through interaction with this factor, as indicated by the high “ σ ”s of
363 these factors.

364 For *MARD*, the results are nearly the same to *SRMSE*. And this means factors behave
365 similarly to these two objective functions.

366

367 Figure 4 gives the sensitivity results based on *SDP* method for *SRMSE*, *WBI*, and *MARD*,
368 from top to bottom. In each plot, the grey and black bars are S_i and S_{Di} for each factor.
369 For *SRMSE*, as indicated by R^2 in the legend, main effects (S_i) contribute to 58.7% of
370 *SRMSE* uncertainty, and quasi total effects (S_{Di}) account for 83% of *SRMSE* uncertainty
371 which is quite high, while other 17% due to higher interactions are not explained. Based
372 on S_{Di} (black bar), the most sensitive factors are $p\gamma$ and $p\kappa$, followed by $p\alpha$ and rCH , and
373 then $p\beta$ and rW_{cmax} while other factors are not sensitive. This result quantitatively
374 corroborates the result obtain from Morris method. The main effects (S_i) of ($p\gamma$, $p\kappa$, and
375 $p\alpha$) are high (i.e., 0.17, 0.18 and 0.14), which suggests these factors should be determined
376 first in model calibration as they lead to the largest reduction in *SRMSE* uncertainty. For
377 each factor, the difference between the black bar and grey bar shows the first order
378 interaction with other factors. This interaction is very strong in $p\gamma$, $p\kappa$, $p\alpha$, and rCH , and
379 very weak in other factors.

380

381 For *WBI*, as indicated by R^2 in the legend, the total main effects (S_i) contribute to 38.4%
382 of the *WBI* uncertainty, quasi total effects (S_{Di}) only account for 57.6% of *WBI*
383 uncertainty, and around 40% due to higher interactions are not explained and can not be
384 ignored. However, by analyzing the result with that from Morris method (top right in
385 Figure 3), we still can get some valuable results: the dominating sensitive factor is $p\kappa$
386 with S_{Di} 0.43 (which is same as Morris method), followed by $p\gamma$, $p\alpha$, and rCH , while
387 other factors are not sensitive; the main effect of $p\kappa$ is as high as 0.27, and it should be

388 fixed in order to get the maximum reduction in *WBI* uncertainty; the first interaction is
389 high in $p\kappa$, $p\gamma$, and $p\alpha$, not obvious in other factors.

390 Similar to the Morris results for *SRMSE* and *MARD*, the result of *MARD* is nearly the
391 same as *SRMSE*. The similar result for *SRMSE* and *MARD* shows similar characteristic
392 relationship between factors and the objective function. This is explainable: a good
393 simulation measured by *SRMSE* will more likely result in a good measure of *MARD*, and
394 vice versa.

395

396 As aforementioned, in the context of multiobjective sensitivity analysis, sensitivity
397 analysis is to exclude the factors which are insensitive to all the objective functions
398 considered. Based on the analysis above, four most insensitive factors are rKs , rKf ,
399 rW_{cmax} , and rW_{gmax} . However, as shown in Figure 4, rW_{cmax} is more sensitive than other
400 three factors, and for objective function *WBI*, as higher order interactions are strong
401 based on SDP (i.e., explains around 40% of model uncertainty), and evaporation is the
402 most sensitive process to water balance (as indicated by $p\kappa$ and rCH) and rW_{cmax} is the
403 only factor related to evaporation storage (Wc), therefore, we only exclude rKf , rKs , and
404 rW_{gmax} for calibration.

405

406 5.2 Multiobjective optimization

407 After sensitivity analysis, only six factors were involved in the calibration. For MOO, we
408 set the initial population size 128 to obtain a good coverage of the factor space and other
409 ϵ -NSGAI parameters to their recommended values, and it led to 482 Pareto front points
410 from totally 22,000 model runs with modified ϵ -NSGAI. And for SOO, it stopped after

411 686 model runs with the classic Nelder–Mead algorithm. Apparently, ϵ -NSGAI took
412 more model simulations than the Nelder–Mead algorithm, but simulation time was
413 compensated by the parallelized code running on high performance clusters.

414

415 Figure 5 shows optimized non-dominant sets normalized within $[0, 1]$ and the black line
416 is for the factor set with SOO. It is encouraging that except rW_{cmax} , factor ranges
417 decreased a lot. This corroborates the conclusion in the sensitivity analysis: $p\gamma$, $p\kappa$, $p\beta$, $p\alpha$,
418 and rC_H are the most sensitive and identifiable factors to these three objective functions,
419 while rW_{cmax} is less sensitive and less identifiable. Several scattered values of $p\gamma$ and
420 dispersed rW_{gmax} show that optimized factor sets are scattered in the response surface
421 rather than concentrated in a continuous region. And the factor set with SOO is within the
422 range of non-dominant sets.

423

424 Figure 6 shows Pareto solutions scattered in the three-dimensional space (top left), and
425 projections in two-dimensional subspaces with corresponding correlation coefficients (r)
426 in the calibration period, with the black dot in each plot denoting the solution for SOO .
427 Correlation coefficients are high and negative for $SRMSE$ and WBI (-0.54), and WBI and
428 $MARD$ (-0.74), and this indicates strong trade-off interactions along the Pareto surface,
429 i.e., better (lower) WBI will eventually result in worse (higher) $SRMSE$, and vice versa.
430 The correlation coefficient is low (0.13) between $SRMSE$ and $MARD$, and is even lower
431 when these two objectives approach to their minima regions (i.e., $SRMSE < 0.53$ and
432 $MARD < 0.09$). This might indicate a poor choice of the objective function, as also shown
433 by similar sensitivity results for these two objective functions in Section 5.1. Table 2 lists

434 the statistics of these three objectives associated with Pareto sets and the result of SOO.
435 For Pareto sets, in the calibration period, the average *SRMSE* is 0.49 ranging from 0.47 to
436 0.57, which corresponds to the average NS 0.78 ranging from 0.67 to 0.78; the average
437 *WBI* is 0.05 ranging from 0.02 to 0.11; and the average *MEAD* is 0.08 ranging from 0.03
438 to 0.11. In the validation period, the average *SRMSE* is 0.54 ranging from 0.51 to 0.62,
439 which corresponds to the average NS 0.70 ranging from 0.61 to 0.74; the average *WBI* is
440 0.05 ranging from 0.04 to 0.09; and the average *MEAD* is 0.10 ranging from 0.08 to 0.13.
441 And for SOO, *SRMSE*, *WBI* and *MEAD* are 0.48, 0.06 and 0.07 for the calibration period,
442 and 0.57, 0.06 and 0.10 for the validation, and accordingly the “NS”s are 0.77 and 0.67,
443 respectively. According to Moriasi et al., 2007 which suggests $NS > 0.75$ and $WBI < 10\%$
444 as excellent modelling of river discharge, all Pareto solutions with MOO and the solution
445 with SOO are close to “excellent” for both calibration and validation periods.

446

447 To better visualize Pareto sets and compare with the result of SOO, the level diagrams are
448 plotted in Figure 7 by applying Euclidean norm (2-norm) to evaluate the distance of each
449 Pareto point to the ideal origin (0,0,0) (ideal values for all three normalized objectives are
450 0). In Figure 7, top three plots are for three objectives and the rest for optimized factors,
451 and the black dot in each plot is the solution for SOO. In the level diagrams, each
452 objective and each factor of a point (corresponding to a Pareto solution) is represented
453 with the same 2-norm value for all the plots. Compared with MOO, obviously, SOO was
454 trapped in the local optima as seen in top-left plot. Another SOO was done with starting
455 point close to the optimum of MOO, and now the optimum of SOO is very close to that
456 of MOO, which means optimization with Nelder-Mead algorithm was dependent of

457 starting point. The 2-norm has a close linear relationship with SRMSE due to values of
458 SRMSE are 5 to 10 times of other two objective functions, and it doesn't have such
459 relationship with other two objectives. The scattering of objectives and factors makes it
460 difficult in decision making to select a single solution because there is not a clear trade-
461 off solution (Blasco et al., 2008). However, compared to SOO, the Pareto solutions from
462 MOO can make decision making easy as it can be converted with expert opinion or some
463 utility function.

464

465 Figures 8 and 9 show simulated and observed flow duration curves and time series flows,
466 respectively, with grey lines denoting the simulations with MOO and black lines with
467 SOO. Generally, all simulations match the observation well for both the duration curve
468 and time series flow for both calibration period and validation period. For the duration
469 curve, simulations from MOO show a wide range in the low flows with frequencies from
470 0.85 to 1.0, which reflects the insensitivity of groundwater process (discussed in the
471 sensitivity analysis, i.e., rK_f is insensitive to these three objectives). Except for this, there
472 is a slight overestimation of flows, large flows during the calibration period with
473 frequencies from 0.2 to 0.1, and median to large flows during the validation period with
474 frequencies from 0.5 to 0.1. This might be due to the uncertainty in the reanalyzed
475 climate data. And the extreme flow with frequency around 0 is underestimated, and this is
476 because we chose the logarithm scale of the observed and simulated flows instead of
477 normal scale when computing objectives SRMSE and MARD. With SOO, the deviation
478 from the observed is larger. Similar conclusions can be drawn from the time series

479 simulations in Figure 9, i.e., the wide ranges of low flow period, and underestimation of
480 flow peaks. Other than this, generally all simulations can mimic the observations.

481

482 Figure 10 shows the time series of watershed average storages (soil storage expressed as
483 soil saturation, and groundwater depth), and fluxes (evaporation, surface runoff and
484 baseflow) associated with MOO (shaded) and SOO (black line). With MOO, soil
485 saturation varies from 0.2 to 1.0 and groundwater from 0 to 120mm. The temporal
486 fluctuation of soil moisture is higher than groundwater, but lower than fluxes in
487 evaporation and surface runoff. And this is true for the solution with SOO except the its
488 ranges of soil saturation and groundwater (groundwater is very close to 0mm). For fluxes
489 with MOO, evaporation and surface runoff have more temporal variation than baseflow,
490 and their magnitudes are larger than baseflow. This applies to fluxes with SOO, and its
491 baseflow is close to 0. This can be confirmed by the De Finetti diagram in Figure 11:
492 with MOO, the average contributions of evaporation, surface runoff, and basedflow are
493 49.3%, 46.1%., and 4.8%, respectively while the contribution of baseflow is very
494 insignificant. And the contribution of baseflow is almost 0 with SOO.

495

496 The result of MOO above is based on a single random seed. The result of MOO with
497 another random seed is similar to the above except that range of rW_{cmax} is narrower
498 (however its effect on the simulation result is limited due to its low sensitivity discussed).

499 Multiple-rand-seed MOO is always appealing, but it might not be practical to fully
500 distributed and physically based models which is normally time-consuming in

501 computation. What one can do is to choose a reliable and robust algorithm based on
502 literature review.

503

504 **6 Conclusion**

505 This study presents a multiobjective sensitivity and optimization approach to calibrate a
506 distributed hydrologic model MOBIDIC with its application in the Davidson watershed
507 for three objective functions (i.e., *SRMSE*, *WBI*, and *MAED*). Results show:

508 1) The two sensitivity analysis techniques are effective and efficient to determine the
509 sensitive processes and insensitive parameters: surface runoff and evaporation are
510 very sensitive processes to all three objective functions, while groundwater
511 recession and soil hydraulic conductivity are not sensitive and were excluded in
512 the optimization.

513 2) For *SRMSE* and *MAED*, all the factors have almost same sensitivities, and a low
514 correlation exists between these two objectives in the non-dominance of Pareto
515 set. This might indicate the poor choice of the objective function.

516 3) Both MOO and SOO achieved acceptable results for both calibration period and
517 validation period, in terms of objective functions and visual match between
518 simulated and observed flows and flow duration curves. For example, with MOO,
519 the average NS is 0.75 ranging from 0.67 to 0.78 in the calibration and 0.70
520 ranging from 0.61 to 0.74 in the validation period.

521 4) In the case study, evaporation and surface runoff shows similar importance to
522 watershed water balance while the contribution of baseflow can be ignored.

523 5) Compared to MOO with ϵ -NSGAI, the application of SOO with the Neld-Mead
524 algorithm was dependent of initial starting point. Furthermore, the Pareto solution
525 provides a better understanding of these conflicting objectives and relations
526 between objectives and parameters, and a better way in decision making.

527

528 **Acknowledgement**

529 *The research was supported by the “Thousand Youth Talents” Plan (Xinjiang Project) and*
530 *the National Basic Research Program of China (973 Program: 2010CB951003). The data*
531 *used in this study were acquired as part of the mission of NASA's Earth Science Division and*
532 *archived and distributed by the Goddard Earth Sciences (GES) Data and Information*
533 *Services Center (DISC). The authors would like to thank Dr Rafael Rosolem and the other*
534 *two anonymous reviewers for valuable comments that substantially improved the manuscript.*

535

536 **References**

- 537 Beven, K., and Binley, A.: The future of distributed models –model calibration and
538 uncertainty prediction, *Hydrological Processes*, 6 (3), 279-298, 1992.
- 539 Bekele, E. G., and Nicklow, J. W.: Multi - objective automatic calibration of SWAT
540 using NSGA - II, *J. Hydrol.*, 341(3-4), 165-176, 2007
- 541 Blasco X., Herrero, J. M., Sanchis, J., and Martínez, M.: A new graphical visualization of
542 n-dimensional Pareto front for decision-making in multiobjective optimization,
543 *Information Sciences* 178, 3908-3924, 2008
- 544 Boyle, D., Gupta, H., and Sorooshian, S.: Toward Improved Calibration of Hydrologic
545 Models: Combining the Strengths of Manual and Automatic Methods, *Water Resour.*
546 *Res.*, 36(12), 3663-3674, 2000.

547 Campolongo, F., Cariboni, J., and Saltelli, A.: An effective screening design for
548 sensitivity analysis of large models, *Environmental Modelling and Software*, 22, 1509-
549 1518, 2007.

550 Campo, L., Caparrini F., and Castelli, F.: Use of multi-platform, multi-temporal remote-
551 sensing data for calibration of a distributed hydrological model: an application in the
552 Arno basin, Italy, *Hydrol. Process.*, 20, 2693-2712, 2006

553 Castelli, F., Menduni, G., Caparrini, F., and MAZZANTI, B.: A distributed package for
554 sustainable water management: A case study in the Arno basin, in: *The Role of*
555 *Hydrology in Water Resources Management (Proceedings of a symposium held on the*
556 *island of Capri, Italy, October 2008)*, IAHS Publ. 327, 2009.

557 Cunge, J.A.: On the subject of a flood propagation method (Muskingum method), *Journal*
558 *of Hydraulics Research*, 7 (2), 205-230, 1969.

559 Deb K., Pratap A., Agarwal S., and Meyarivan T.: A fast and elitist multiobjective
560 genetic algorithm: NSGA-II, *IEEE Trans Evol Comput*, 6(2), 182–97, 2002.

561 Efstratiadis, A. and Koutsoyiannis, D.: One decade of multi-objective calibration
562 approaches in hydrological modelling: a review, *Hydrol. Sci. J.*, 55(1), 58–78, 2010

563 Gupta, H., S. Sorooshian, and Yapo, P.: Toward Improved Calibration of Hydrologic
564 Models: Multiple and Noncommensurable Measures of Information, *Water Resour.*
565 *Res.*, 34(4), 751-763, 1998.

566 Kollat J.B., and Reed P.: Comparing state-of-the-art evolutionary multiobjective
567 algorithms for long-term groundwater monitoring design, *Adv Water Resour*, 29(6),
568 792-807, 2006.

569 Kollat, J.B., and Reed, P.: A framework for visually interactive decision-making and
570 design using evolutionary multi-objective optimization (VIDEO), *Environmental*
571 *Modelling & Software*, 22(12), 1691-1704, 2007.

572 Kumar, S.V., Peters-Lidard, C.D., Tian, Y., Houser, P.R., Geiger, J., Olden, S., Lighty, L.,
573 Eastman, J.L., Doty, B., Dirmeyer, P., Adams, J., Mitchell, K., Wood, E.F., and
574 Sheffield, J.: Land Information System – An Interoperable Framework for High
575 Resolution Land Surface Modeling, *Environ. Mod. & Soft.*, 21, 1402-1415, 2006.

576 Liu, Y., and Sun, F.: Sensitivity analysis and automatic calibration of a rainfall–runoff
577 model using multiobjectives, *Ecological Informatics*, 5, 304-310, 2010.

578 MacLean, A.J., Tolson, B.A., Seglenieks, F.R., and Soulis, E.: Multiobjective calibration
579 of the MESH hydrological model on the Reynolds Creek Experimental Watershed,
580 *Hydrol. Earth Syst. Sci. Discuss.*, 7, 2121-2155, 2010.

581 Madsen H.: Automatic calibration of a conceptual rainfall–runoff model using multiple
582 objectives, *Journal of Hydrology*, 235, 276-88, 2000.

583 Madsen, H.: Parameter estimation in distributed hydrological catchment modelling using
584 automatic calibration with multiple objectives, *Advances in Water Resources*, 26(2),
585 205-216, 2003.

586 Moriasi, D., Arnold, J., Van Liew, M., Bingner, R., Harmel, R., and Veith, T.: Model
587 evaluation guidelines for systematic quantification of accuracy in watershed
588 simulations, *T. ASABE.*, 50, 885-900, 2007.

589 Morris, M.D.: Factorial sampling plans for preliminary computational experiments,
590 *Technometrics* 33 (2), 161-174, 1991.

591 Muleta, M.K., and Nicklow, J.W.: Sensitivity and uncertainty analysis coupled with
592 automatic calibration for a distributed watershed model, *Journal of Hydrology*, 306,
593 127-145, 2005.

594 Nash, J. E., and Sutcliffe, J. V.: River flow forecasting through conceptual models part I
595 — A discussion of principles, *Journal of Hydrology*, 10 (3), 282–290, 1970.

596 Nelder, J.A., and Mead, R.: A simplex method for function minimization, *Computer*
597 *Journal*, 7, 308-313, 1965.

598 Peters-Lidard, C.D., Houser, P.R., Tian, Y., Kumar, S.V., Geiger, J., Olden, S., Lighty, L.,
599 Doty, B., Dirmeyer, P., Adams, J., Mitchell, K., Wood, E.F. and Sheffield, J.: High-
600 performance Earth system modeling with NASA/GSFC's Land Information System,
601 *Innov. Sys. and Soft. Eng.*, 3(3), 157-165, 2007.

602 Refsgaard, J.C., and Storm, B.: MIKE SHE, in: *Computer Models in Watershed*
603 *Hydrology*, edited by Singh, V.J., Water Resour. Publications, Rome, Italy, pp. 809-
604 846, 1995

605 Ratto, M., Pagano, A., and Young, P.: State dependent parameter meta-modelling and
606 sensitivity analysis, *Computer Physics Communications*, 177, 863-876, 2007.

607 Rosolem, R., Gupta, H.V., Shuttleworth, W.J., Zeng, X., and Gonçalves, L.G.G.: A fully
608 multiple-criteria implementation of the Sobolj method for parameter sensitivity
609 analysis, *Journal of Geophysical Research: Atmospheres (1984–2012)*, 117(D7), 2012.

610 Rosolem, R., Gupta, H.V., Shuttleworth, W.J., Gonçalves, L.G.G., and Zeng, X.:
611 Towards a comprehensive approach to parameter estimation in land surface
612 parameterization schemes, *Hydrological Processes*, 27(14), 2075-2097, 2013.

613 Shafii M., and De Smedt, F.: Multiobjective calibration of a distributed hydrological
614 model (WetSpa) using a genetic algorithm, *Hydrology and Earth system sciences*, 13,
615 2137-2149, 2009.

616 Saltelli, A., Ratto, M., Andres, T., Campolongo, F., Cariboni, J., Gatelli, D., Saisana, M.,
617 and Tarantola, S.: *Global Sensitivity Analysis, The Primer*. Wiley & Sons, Chichester,
618 United Kingdom, 2008.

619 Saltelli, A., and Annoni, P.: How to avoid a perfunctory sensitivity analysis,
620 *Environmental Modelling and Software*, 25(12), 1508-1517, 2010.

621 Tang, Y., Reed, P., and Wagener, T.: How effective and efficient are multiobjective
622 evolutionary algorithms at hydrologic model calibration? *Hydrol. Earth Syst. Sci.*,
623 10:289–307, 2006.

624 Van Werkhoven, K., Wagener, T., Reed, P., and Tang, Y.: Sensitivity-guided reduction
625 of parametric dimensionality for multi-objective calibration of watershed models,
626 *Advances in Water Resources*, 32(8), 1154-1169, 2009.

627 Vrugt, J., Gupta, H. V., Bastidas, L. A., Bouten, W., and Sorooshian, S.: Effective and
628 efficient algorithm for multiobjective optimization of hydrologic models, *Water*
629 *Resour. Res.*, 39, 1214, doi:1210.1029/2002WR001746, 2003.

630 Wöhling, T., Barkle, G.F., and Vrugt, J.A.: Comparison of three multiobjective
631 optimization algorithms for inverse modeling of vadose zone hydraulic properties, *Soil*
632 *Science Society of America Journal*, 72(2), 305-319, 2008

- 633 Yang, J., Reichert, P., Abbaspour, K.C., and Yang, H.: Hydrological modelling of the
634 Chaohe Basin in China: statistical model formulation and Bayesian inference, Journal
635 of Hydrology 340, 167-182, 2007.
- 636 Yang, J.: Convergence and uncertainty analyses in Monte-Carlo based sensitivity analysis,
637 Environmental Modelling & Software 26, 444-457, 2011.
- 638 Yapo P.O., Gupta H.V., and Sorooshian S.: Multiobjective global optimization for
639 hydrologic models, Journal of Hydrology 204, 83-97, 1998
- 640 Zitzler E, Laumanns M., and Thiele L.: SPEA2: improving the strength Pareto
641 evolutionary algorithm, Tech Rep TIK-103, Department of Electrical Engineering,
642 Swiss Federal Institute of Technology, 2001.

Table 1 Initial selected factors, initial estimation of the corresponding MOBIDIC parameter, and factor ranges

Factor	Meaning of the given factor	Initial estimation of MOBIDIC parameter	Factor range
$p\gamma$	Exponential change ^{*1} on soil percolation coefficient γ [s^{-1}]	1.2e-011	[-2, 9]
$p\kappa$	Exponential change on soil adsorption coefficient κ [s^{-1}]	1.6e-007	[-6, 5]
$p\beta$	Exponential change on interflow coefficient β [s^{-1}]	2.5e-006	[-7, 4]
$p\alpha$	Exponential change on surface storage decay coefficient α [s^{-1}]	3.3e-007	[-6, 5]
rK_s	Multiplying change ^{*2} on soil hydraulic conductivity [m/s]	[5.0e-006, 8.9e-005]	[0.001, 100]
rW_{cmax}	Multiplying change on maximum storage of the capillary reservoir [m]	[0.017, 0.165]	[0.01, 5]
rW_{gmax}	Multiplying change on maximum storage of the gravitational reservoir [m]	[0.107, 0.449]	[0.01, 5]
rC_H	Multiplying change on bulk turbulent exchange coefficient for heat [-]	[0.010, 0.018]	[0.01, 5]
rK_f	Multiplying change on groundwater decay coefficient [s^{-1}]	1.0e-007	[0.001, 5]

*1 Exponential change pX means the corresponding MOBIDIC parameter X will be changed according to $X = X_0 \times \exp(pX - 1)$, where X_0 is the initial estimation of X ;

*2 Multiplying change rX means the corresponding MOBIDIC parameter X will be changed according to $X = X_0 \times rX$

Table 2 Statistics of three objective functions associated with multiobjective optimization and single objective optimization

	Multiobjective optimization						Single objective optimization	
	Calibration			Validation			Calibration	Validation
	Mean	Min	Max	Mean	Min	Max		
<i>SRMSE</i>	0.49	0.47	0.57	0.54	0.51	0.62	0.48	0.57
<i>WBI</i>	0.05	0.02	0.11	0.05	0.04	0.09	0.07	0.06
<i>MAED</i>	0.08	0.03	0.11	0.10	0.08	0.13	0.07	0.10

Figure Captions

Figure 1 A schematic representation of MOBIDIC. Boxes denote different water storages (gravitational storage W_g , capillary storage W_c , groundwater storage H , surface storage W_s , and river system), solid arrows fluxes (evaporation E_t , precipitation P , infiltration I_{nf} , adsorption A_d , percolation P_c , surface runoff R , interflow Q_d , groundwater discharge Q_g , and surface runoff and interflow from upper cells $(R+Q_d)_{up}$), dashed arrows different routings, and blue characters major model parameters.

Figure 2 The location of Davidson watershed, North Carolina, with DEM map, river system (lines), and watershed outlet (the triangle point)

Figure 3 Multiobjective sensitivity analysis result based on the Morris method (μ is the sensitivity measure, and σ demonstrates the degree of nonlinearity or factor interaction)

Figure 4 Multiobjective sensitivity analysis result based on the SDP method

Figure 5 The normalized factor sets associated with MOO (grey lines) and the solution with SOO (dark line)

Figure 6 The Pareto solutions in the three dimensional space (top left), and the projections in the two dimensional subspace (other plots), with MOO, and the black dot is the solution with SOO

Figure 7 2-norm level diagrams representation of the Pareto sets with MOO, and the solution with SOO (black dot)

Figure 8 Flow duration curve for observed (dotted line), and simulated with MOO (grey) and SOO (solid line)

Figure 9 Observed flows (dotted) and simulated flows with MOO (grey) and SOO (black line) for the calibration period (top) and validation period (bottom)

Figure 10 Time series of watershed average storages (soil water storage expressed as soil saturation, and groundwater depth), and fluxes (evaporation, surface runoff, and baseflow) with MOO (grey) and SOO (black line). For SOO, the groundwater storage and baseflow are close to 0 and hardly seen.

Figure 11 De Finetti diagram (Ternary plot) of Evaporation, Surface runoff, and Baseflow with MOO (grey) and SOO (black star)

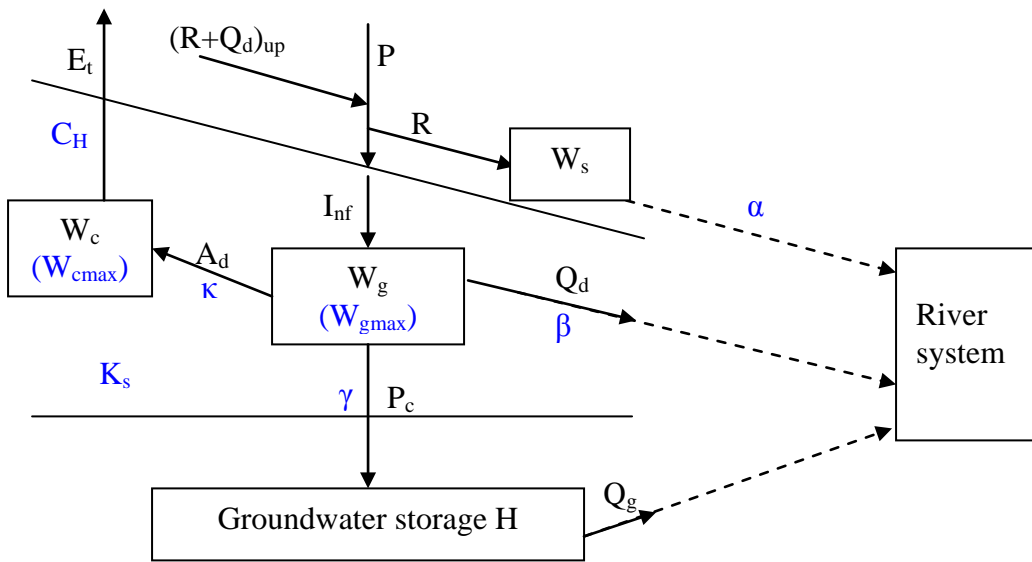


Figure 1 A schematic representation of MOBIDIC. Boxes denote different water storages (gravitational storage W_g , capillary storage W_c , groundwater storage H , surface storage W_s , and river system), solid arrows fluxes (evaporation E_t , precipitation P , infiltration I_{nf} , adsorption A_d , percolation P_c , surface runoff R , interflow Q_d , groundwater discharge Q_g , and surface runoff and interflow from upper cells $(R+Q_d)_{up}$), dashed arrows different routings, and blue characters major model parameters.

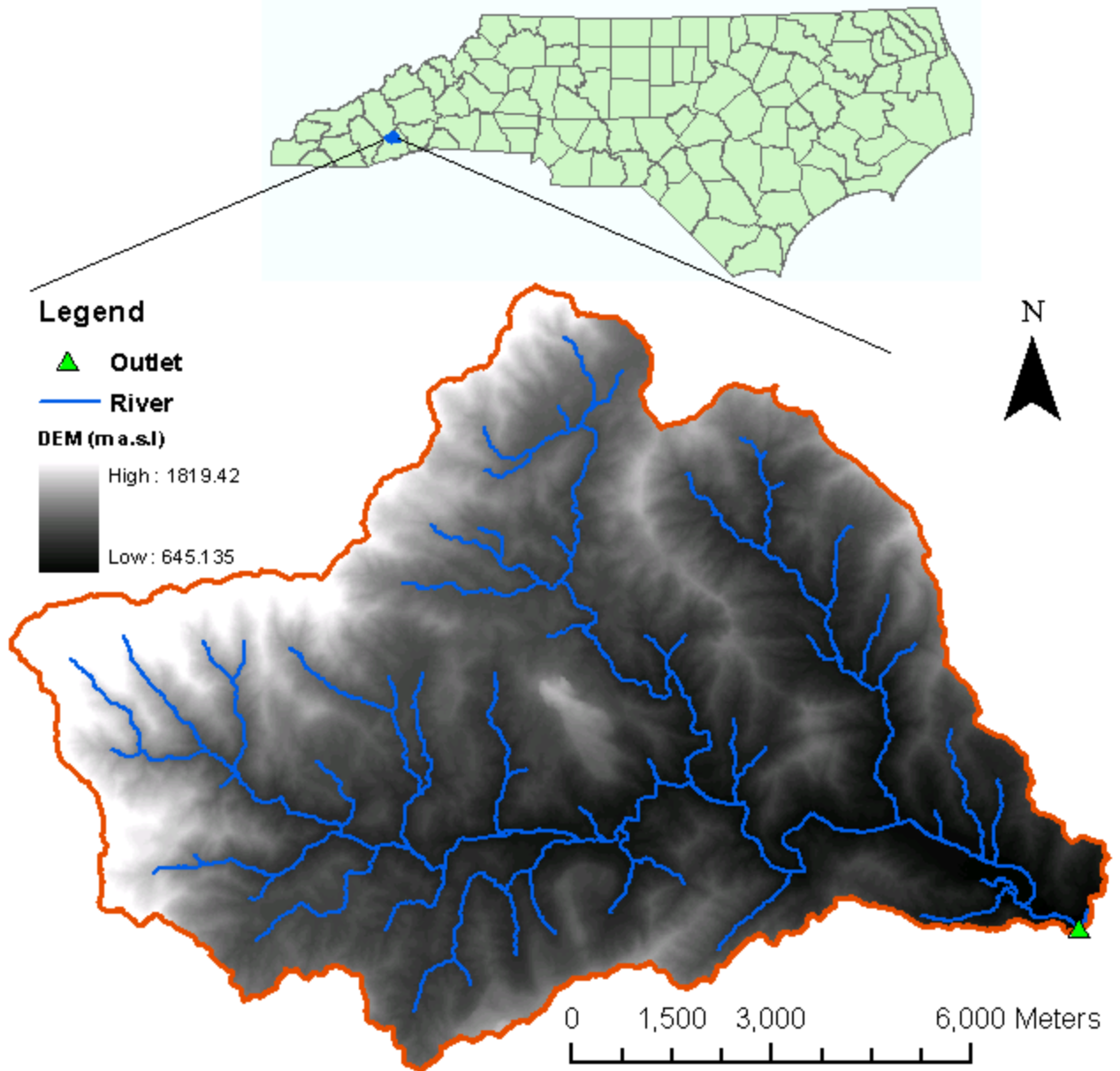


Figure 2 The location of the Davidson watershed, North Carolina, with DEM map, river system (lines), and watershed outlet (the triangle point)

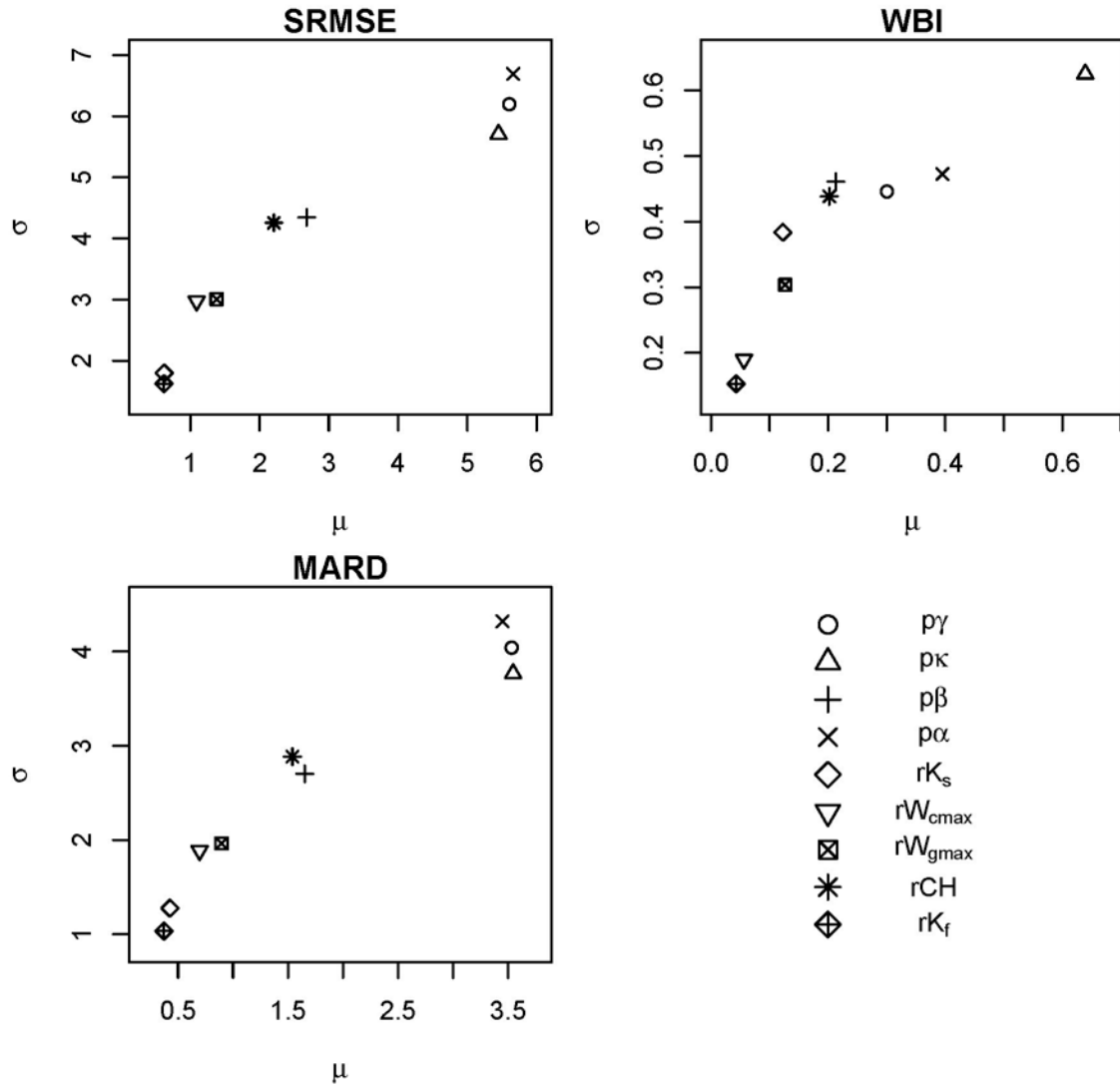


Figure 3 Multiobjective sensitivity analysis result based on the Morris method (μ is the sensitivity measure, and σ demonstrates the degree of nonlinearity or factor interaction)

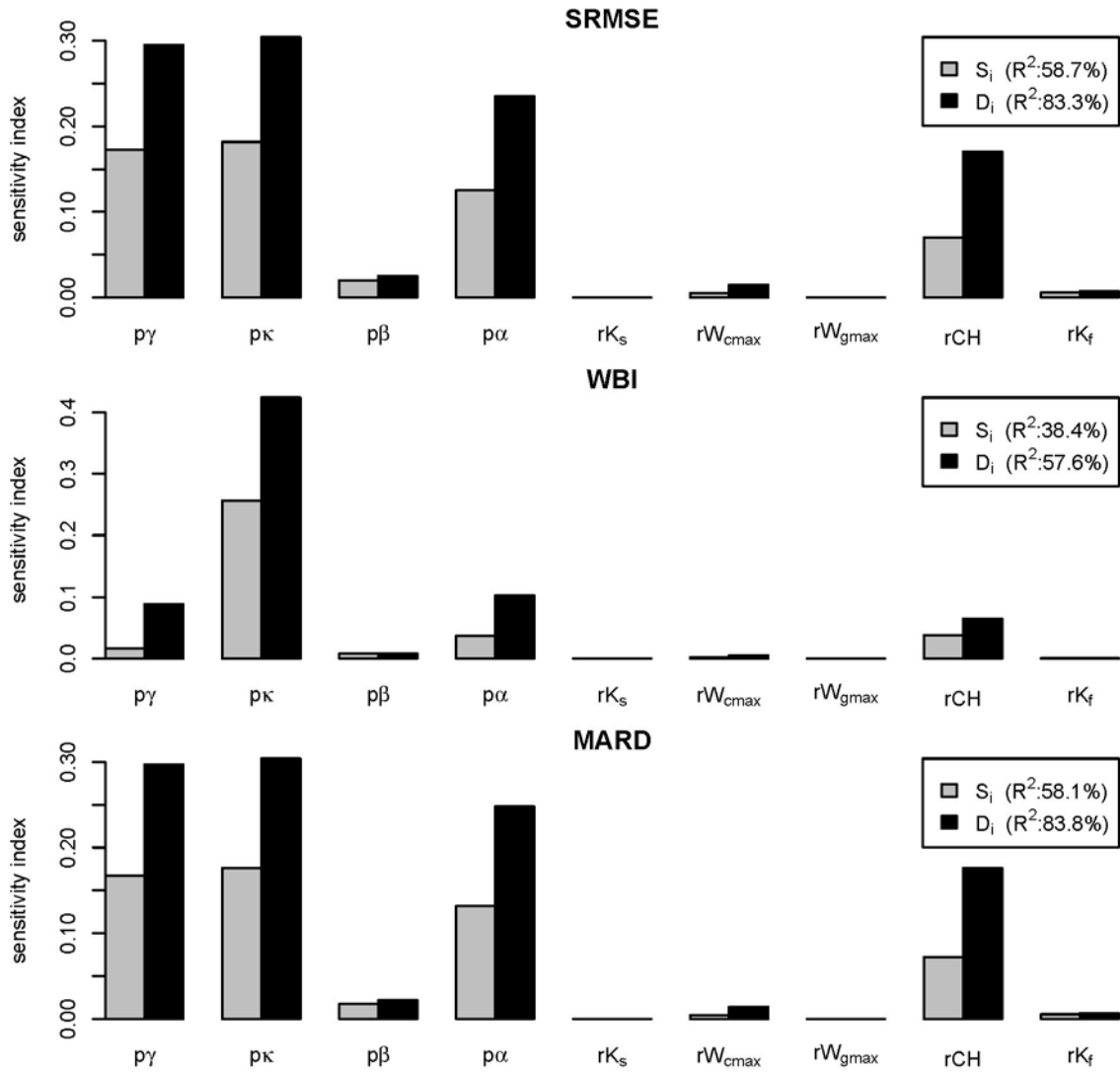


Figure 4 Multiobjective sensitivity analysis result based on the SDP method

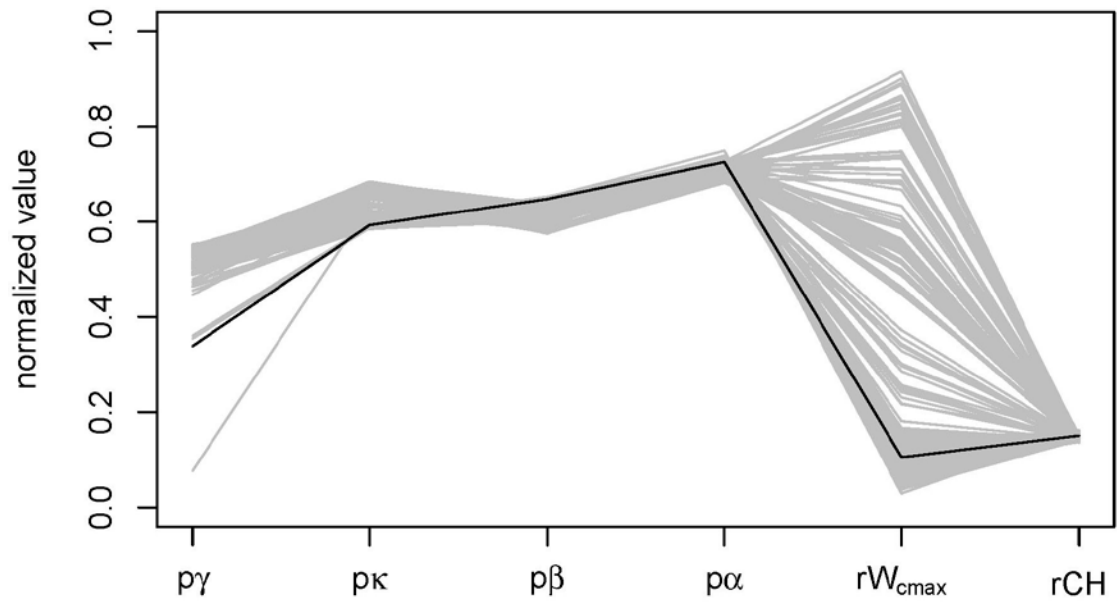


Figure 5 The normalized factor sets corresponding to the Pareto solutions (grey lines) with MOO and the solution with SOO (dark line)

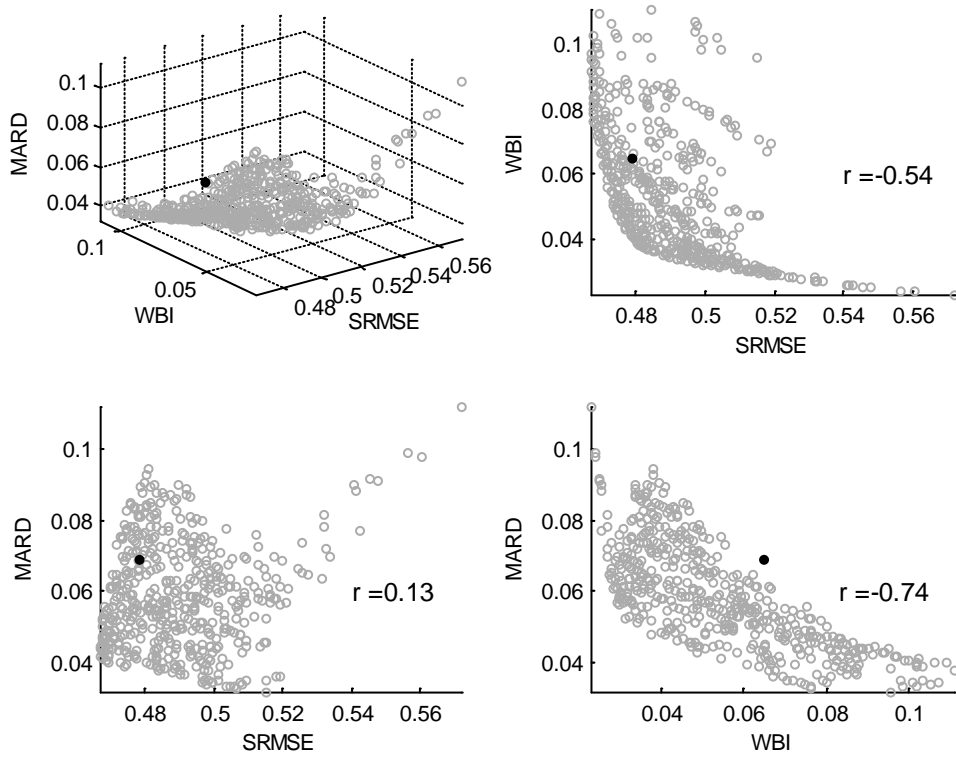


Figure 6 The Pareto solutions in the three dimensional space (top left), and the projections in the two dimensional subspace (other plots), with MOO, and the black dot is the solution with SOO

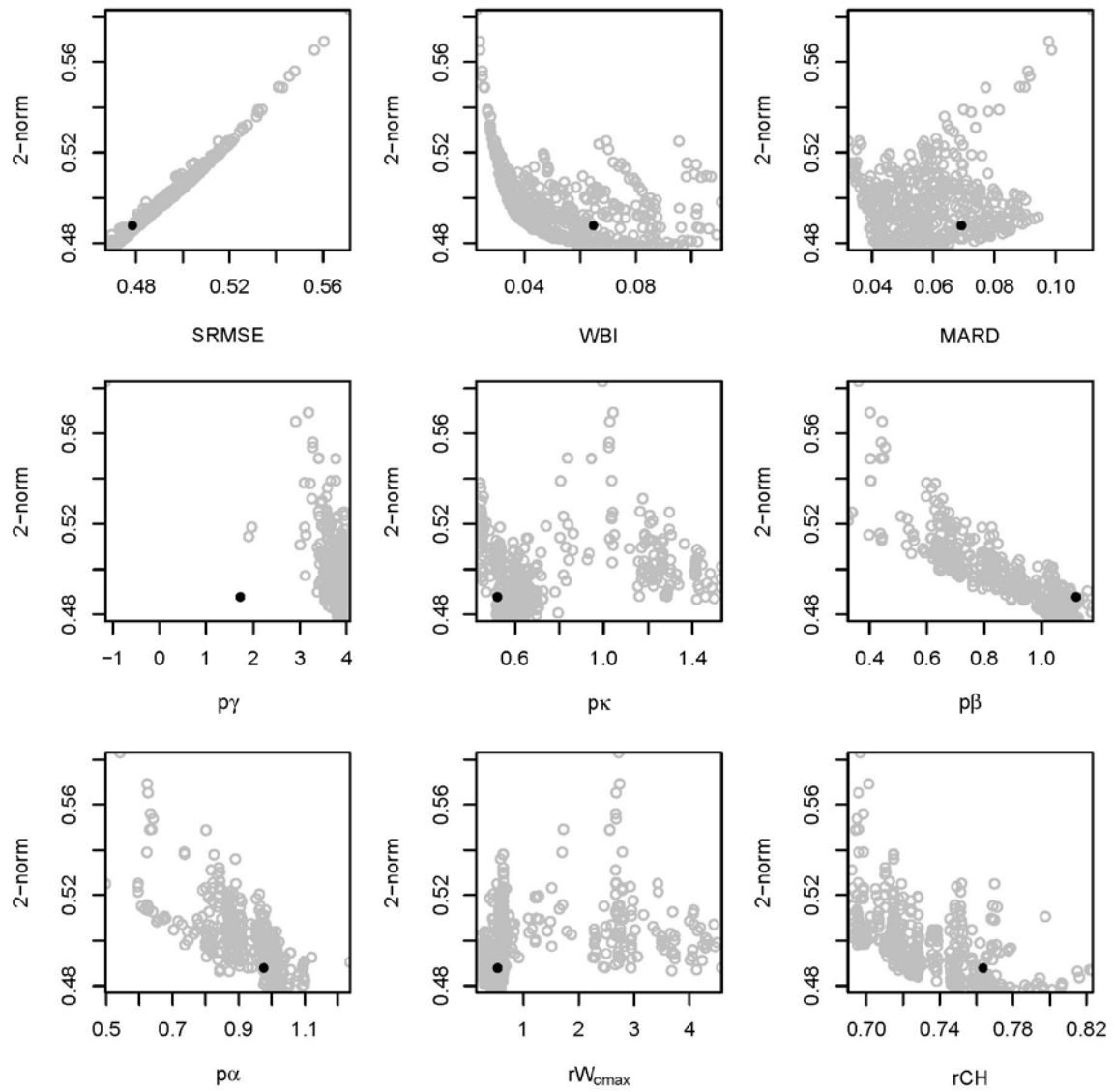


Figure 7 2-norm level diagrams representation of the Pareto sets with MOO, and the solution with SOO (black dot)

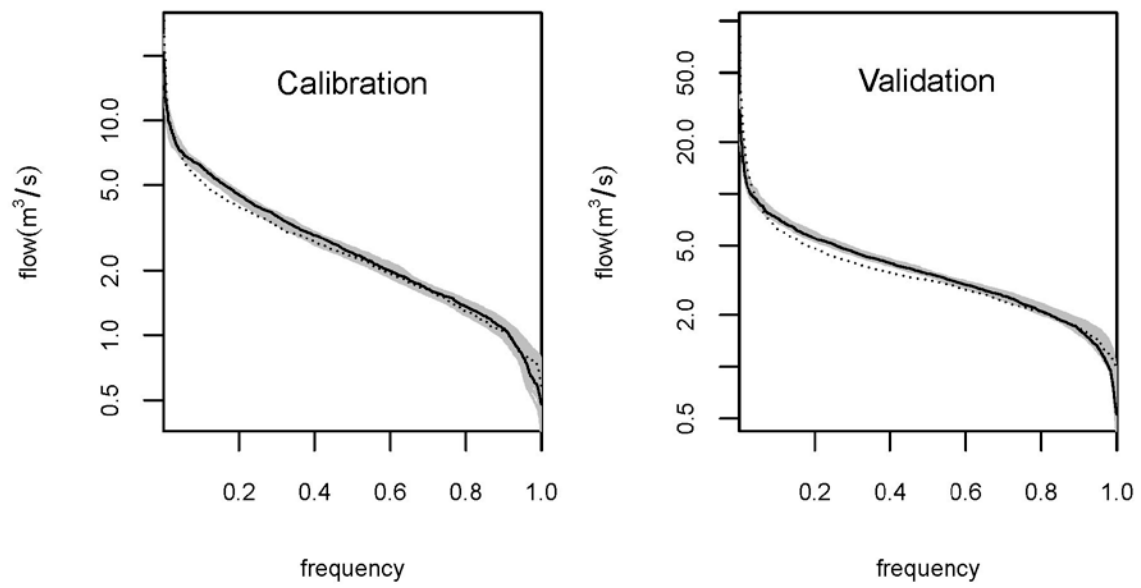


Figure 8 Flow duration curve for observed (dotted line), and simulated with MOO (grey) and SOO (solid line)

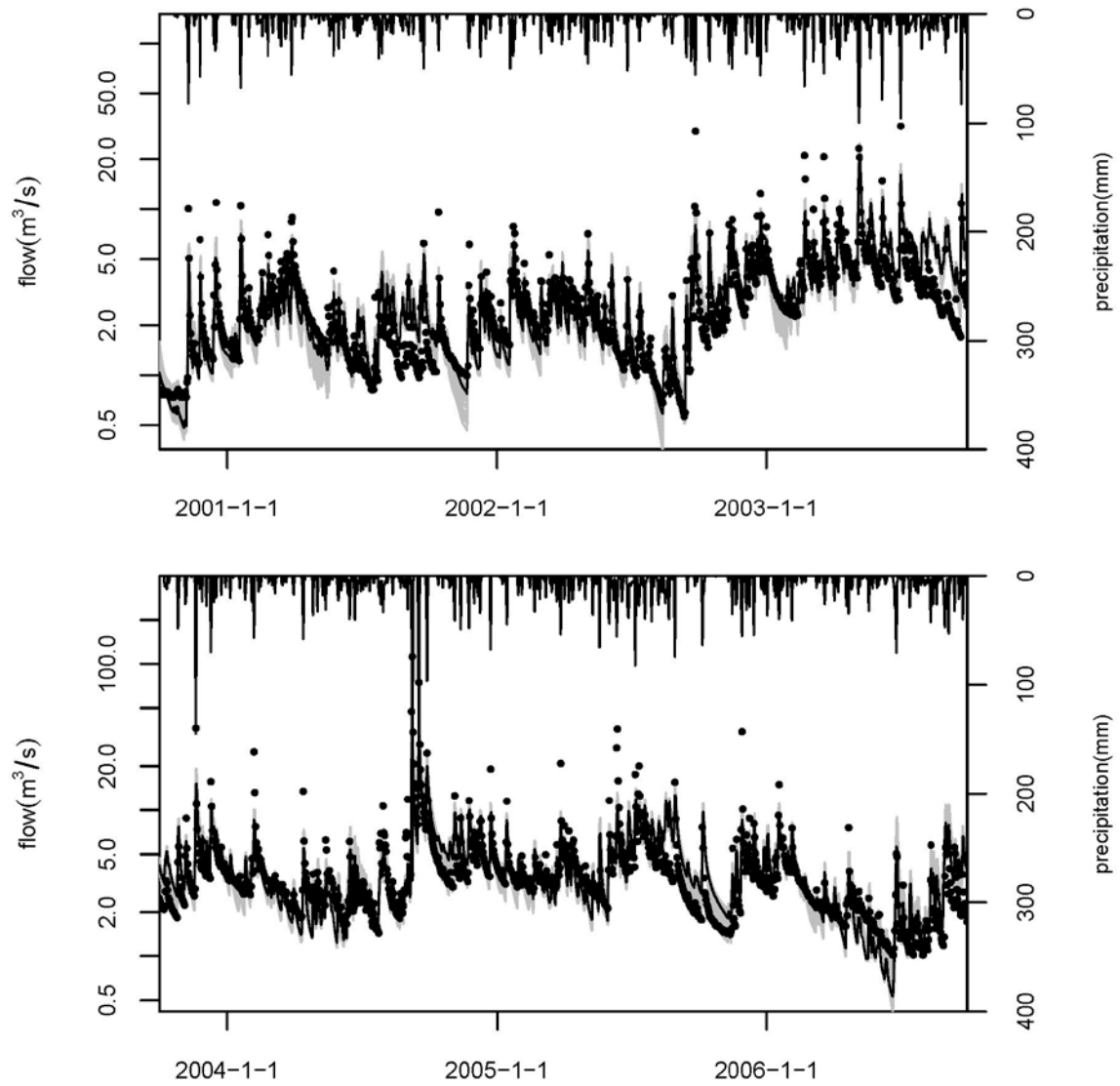


Figure 9 Observed flows (dotted) and simulated flows with MOO (grey) and SOO (black line) for the calibration period (top) and validation period (bottom)

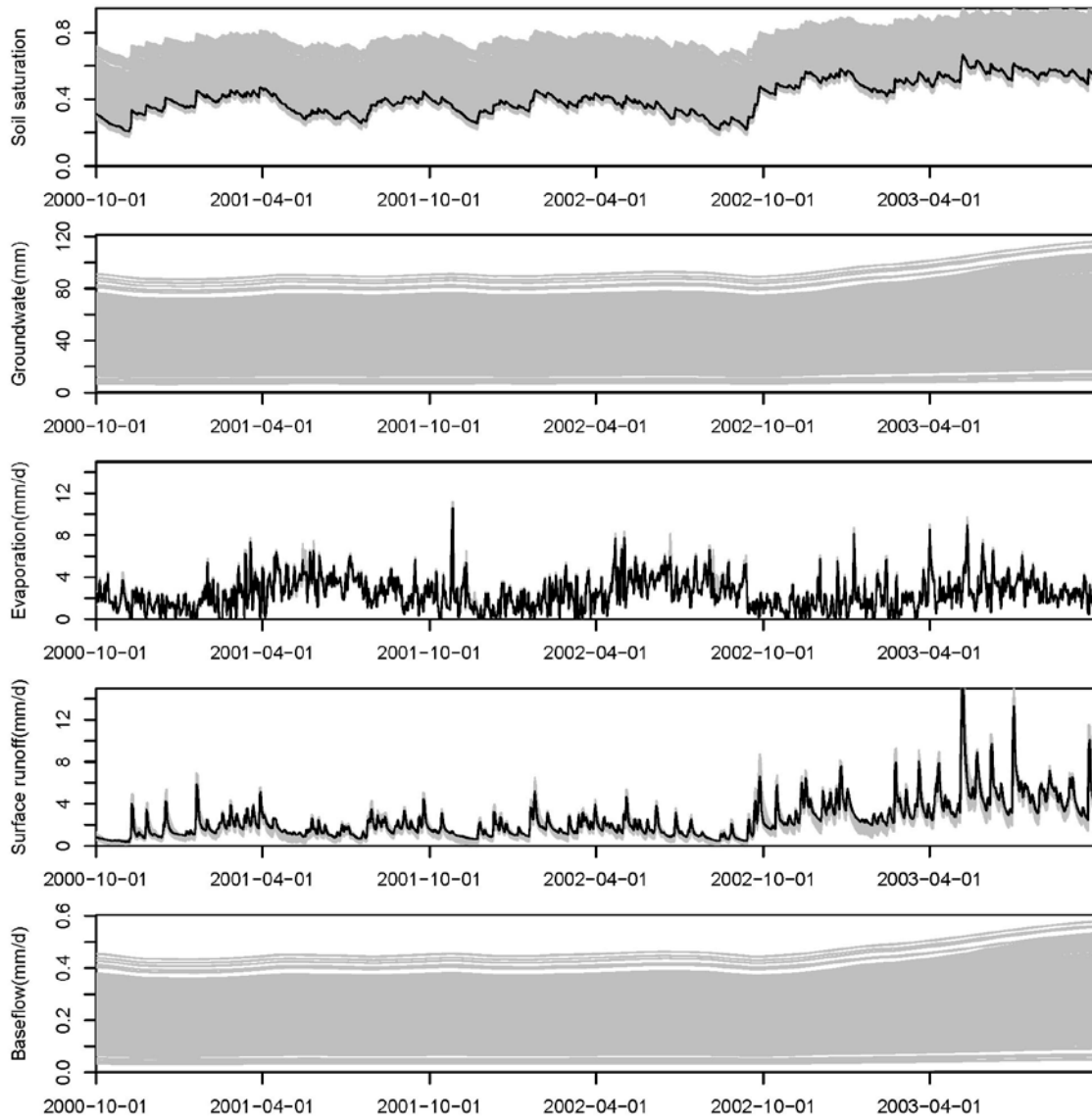


Figure 10 Time series of watershed average storages (soil water storage expressed as soil saturation, and groundwater depth), and fluxes (evaporation, surface runoff, and baseflow) with MOO (grey) and SOO (black line). For SOO, the groundwater storage and baseflow are close to 0 and hardly seen.

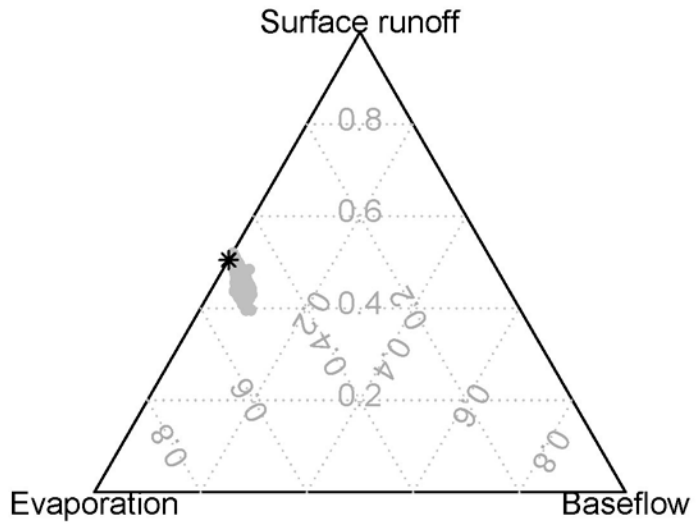


Figure 11 De Finetti diagram (Ternary plot) of Evaporation, Surface runoff, and Baseflow with MOO (grey) and SOO (black star)